FRONTIERS OF PHYSICS

RESEARCH ARTICLE
Volume 19 / Issue 3 / 31201 / 2024

Preparation of maximally-entangled states with multiple cat-state qutrits in circuit QED

Chui-Ping Yang[1], Jia-Heng Ni[1], Liang Bin[1], Yu Zhang[2], Yang Yu[2], Qi-Ping Su[1,3,†]

1 Department of Physics, Hangzhou Normal University, Hangzhou 311121, China
2 School of Physics, Nanjing University, Nanjing 210093, China
3 Institute for Quantum Science and Technology, University of Calgary, Alberta T2N 1N4, Canada
Corresponding author. E-mail: †sqp@hznu.edu.cn
Received June 27, 2023; accepted October 11, 2023

ABSTRACT

In recent years, cat-state encoding and high-dimensional entanglement have attracted much attention. However, previous works are limited to generation of entangled states of cat-state qubits (two-dimensional entanglement with cat-state encoding), while how to prepare entangled states of cat-state qutrits or qudits (high-dimensional entanglement with cat-state encoding) has not been investigated. We here propose to generate a maximally-entangled state of multiple cat-state qutrits (three-dimensional entanglement by cat-state encoding) in circuit QED. The entangled state is prepared with multiple microwave cavities coupled to a superconducting flux ququart (a four-level quantum system). This proposal operates essentially by the cavity-qutrit dispersive interaction. The circuit hardware resource is minimized because only a coupler ququart is employed. The higher intermediate level of the ququart is occupied only for a short time, thereby decoherence from this level is greatly suppressed during the state preparation. Remarkably, the state preparation time does not depend on the number of the qutrits, thus it does not increase with the number of the qutrits. As an example, our numerical simulations demonstrate that, with the present circuit QED technology, the high-fidelity preparation is feasible for a maximally-entangled state of two cat-state qutrits. Furthermore, we numerically analyze the effect of the inter-cavity crosstalk on the scalability of this proposal. This proposal is universal and can be extended to accomplish the same task with multiple microwave or optical cavities coupled to a natural or artificial four-level atom.

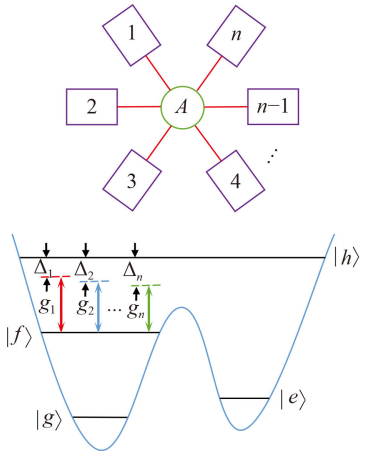

Keywords maximally-entangled states, cat state, qutrit, circuit QED

1 Introduction and motivation

Quantum computing and communication outperform classical computing and communication in specific problems [1–3]. They have made rapid progress in practical applications. The study of quantum computing and communication has mainly focused on two-dimensional systems, namely qubits. However, compared with a qubit, a qudit (i.e., d-dimensional system) can be used to encode more information in quantum computing and communication. In the family of qudits, qutrits (i.e., three-dimensional systems) are the closest members to qubits. Recently, quantum entangled states in qutrits or higher-dimensional systems have attracted much atten-

Higher Education Press

https://doi.org/10.1007/s11467-023-1357-4

tion. They have many important applications, such as improving the security of quantum key distribution [4], simplifying quantum logic [5], increasing the generation rate of quantum random numbers [6], and testing the compatibility-loophole-free contextuality [7]. A number of works have been devoted to producing entangled states with qutrits or higher-dimensional systems by using various degrees of freedom of light or photons [8–17].

Encoding quantum information onto bosonic systems is a promising route to quantum error correction and fault-tolerant quantum computation. In a cat-state qubit (qubit encoded by cat states), this encoding relies on the confinement of the system's dynamics onto the two-dimensional manifold spanned by two orthogonal or quasi-orthogonal Schrödinger cat states. Cat-state qubits have attracted extensive attention thanks to their enhanced lifetimes [18]. Recently, there has been an increasing interest in quantum computing with cat-state qubits. Many efforts have been made towards the generation of cat states [19–22]. Schemes have been presented for creating entanglement among multiple cat-state qubits [23–26]. Moreover, proposals have been put forward for realizing quantum gates with a single cat-state qubit [27–29], quantum gates with two cat-state qubits [30, 31], and quantum gates with multiple cat-state qubits [32]. Furthermore, experiments have demonstrated quantum gates of a single cat-state qubit [33, 34] and created Bell states of two cat-state qubits [35, 36]. However, after a deep search of literature, we found that the previous works are limited to generation of entangled states of cat-state qubits (two-dimensional entanglement with cat-state encoding), while how to prepare entangled states of cat-state qutrits or qudits (high-dimensional entanglement with cat-state encoding) has not be reported yet.

Circuit QED is an analogue of cavity QED, which consists of microwave resonators (or cavities) and superconducting (SC) qubits. Circuit QED is a highly controllable platform for quantum state manipulation and is considered as one of the most promising candidates for quantum computing and quantum information processing [37–43]. SC qubits have the flexibility in both fabrication and controlling of their level spacings. Their coherence times have been significantly improved recently [44–48]. These features allow SC qubits to be designed and fabricated in various kinds of spatial structures and to be used as good information carriers and units of quantum information processors. On the other hand, superconducting microwave cavities or resonators are of particular interest due to their high performance to mediate nonlocal interactions between adjacent or non-adjacent SC qubits in integrated quantum circuits [37–43]. Moreover, it has been commonly recognized that a superconducting microwave cavity with a high quality factor can be utilized as a good quantum memory [49, 50], because it hosts microwave photons with a much longer lifetime than SC qubits [51]. In recent years, there is an increasing interest in quantum state engineering and quantum computing with microwave fields or photons.

Motivated by the above, this work focuses on the generation of entangled state of multiple cat-state qutrits (three-dimensional entanglement with cat-state encoding) based on circuit QED. Specifically, we will propose an approach to prepare multiple cat-state qutrits in the following maximally-entangled state

$$\frac{1}{\sqrt{3}}\left(|C_0\rangle|C_0\rangle\cdots|C_0\rangle+|C_1\rangle|C_1\rangle\cdots|C_1\rangle+|C_2\rangle|C_2\rangle\cdots|C_2\rangle\right), \tag{1}$$

where (from left to right) the first $\{|C_0\rangle,|C_1\rangle,|C_2\rangle\}$ are the three cat states of the first qutrit, the second $\{|C_0\rangle,|C_1\rangle,|C_2\rangle\}$ are the three cat states of the second qutrit, while the last $\{|C_0\rangle,|C_1\rangle,|C_2\rangle\}$ are the three cat states of the last qutrit. The expressions of the three cat states are

$$\begin{aligned}
|C_0\rangle &= \mathcal{N}_0\left(|\alpha\rangle+|-\alpha\rangle\right),\\
|C_1\rangle &= \mathcal{N}_1\left(|\alpha e^{i\pi/3}\rangle+|-\alpha e^{i\pi/3}\rangle\right),\\
|C_2\rangle &= \mathcal{N}_2\left(|\alpha e^{i2\pi/3}\rangle+|-\alpha e^{i2\pi/3}\rangle\right).
\end{aligned} \tag{2}$$

Here, $\mathcal{N}_0$, $\mathcal{N}_1$, and $\mathcal{N}_2$ are normalization coefficients with $\mathcal{N}_0=\mathcal{N}_1=\mathcal{N}_2=1/\sqrt{2\left(1+e^{-2|\alpha|^2}\right)}$. For the three cat states being the three logic states of each qutrit, the three cat states require to be orthogonal or quasi-orthogonal. Note that this condition can be met for $|\alpha|\geq 2.2$. This is because: with the chosen value of α here, one can easily verify $|\langle C_m|C_n\rangle|^2<10^{-3}$ $(m,n\in\{0,1,2\},\ m\neq n)$, which is a good condition that any two of the three cat states can be considered as quasi-orthogonal. Note that the three cat states given in Eq. (2) form a three-dimensional Hilbert space for a cat-state qutrit. Accordingly, the entangled state given in Eq. (1) is a three-dimensional maximally-entangled state of multiple cat-state qutrits.

The entangled state (1) is prepared by employing multiple microwave cavities coupled to a SC flux ququart (a four-level quantum system). The proposal operates essentially by the qutrit-cavity dispersive interaction. As shown below, this proposal has the following advantages: (i) Because only a coupler ququart is employed, the circuit hardware resource is minimized; (ii) Since the higher intermediate level of the ququart is occupied only for a short time, decoherence from this level of the ququart is greatly suppressed during the state preparation; (iii) Interestingly, the state preparation time does not depend on the number of the qutrits, thus it does not increase with the number of the qutrits. As an example, we further discuss the experimental feasibility for preparing a maximally entangled state of two cat-state qutrits based on circuit QED. This proposal is universal and can be extended to generate the maximally-entangled state of multiple cat-state qutrits, by

employing multiple microwave or optical cavities coupled to a natural or artificial four-level atom. To the best of our knowledge, this work is the first to produce entangled states with cat-state qutrits based on circuit or cavity QED.

Compared to entangled states of cat-state qubits (two-dimensional entanglement), the entangled state (1) exhibits higher-dimensional entanglement due to its involvement of cat-state qutrits. Therefore, the entangled state (1) is inherently significant in the field of quantum physics. It holds particular importance in high-dimensional quantum computing and high-dimensional quantum error correction, where information is encoded using cat-state qutrits. Furthermore, this state could serve as a quantum channel for establishing quantum networks to implement various quantum communication tasks, such as teleportation, quantum key distribution, superdense encoding, and networked credit account opening.

This paper is arranged as follows. In Section 2, we derive an effective Hamiltonian. In Section 3, we explicitly show how to prepare the maximally-entangled state of multiple cat-state qutrits based on circuit QED. In Section 4, we numerically analyze the circuit-QED experimental feasibility for creating a maximally-entangled state of two cat-state qutrits and also discuss the effect of the inter-cavity crosstalk on the scalability of this proposal. A brief conclusion is given in Section 5.

2 Effective Hamiltonian

Consider a setup consisting of n microwave cavities $(1,2,\cdots,n)$ coupled to a SC flux ququart [Fig. 1(a)]. The four levels of the flux ququart are denoted as $|g\rangle$, $|e\rangle$, $|f\rangle$, and $|h\rangle$ [Fig. 1(b)]. In general, there exists the transition between the two lowest levels $|g\rangle$ and $|e\rangle$. However, this transition can be made to be weak by increasing the barrier between the two potential wells. Therefore, the coupling of the $|g\rangle \leftrightarrow |e\rangle$ transition with the n cavities can be assumed negligible during the entangled state preparation. Note that the coupling and decoupling of the flux ququart from the n cavities can be achieved by adjusting the level spacings of the flux ququart. For superconducting devices, their level spacings can be rapidly (within 1–3 ns) adjusted by changing external control parameters [52, 53].

Adjust the level spacings of the ququart such that the n cavities $(1,2,\cdots,n)$ are dispersively coupled to the $|f\rangle \leftrightarrow |h\rangle$ transition, while highly detuned (decoupled) from the transitions between any other two levels [Fig. 1(b)]. In the interaction picture and after applying the rotating-wave approximation (RWA), one has

$$H_I = \sum_{j=1}^{n} g_j \left(\mathrm{e}^{\mathrm{i}\Delta_j t} a_j |h\rangle\langle f| + \mathrm{h.c.}\right), \tag{3}$$

where a_j is the annihilation operator for the mode of cavity j, g_j is the coupling constant between cavity j and the $|f\rangle \leftrightarrow |h\rangle$ transition of the ququart, and $\Delta_j = \omega_{hf} - \omega_{c_j}$ is the detuning between the frequency ω_{c_j} of cavity j and the $|f\rangle \leftrightarrow |h\rangle$ transition frequency ω_{hf} of the ququart $(j = 1,2,\cdots,n)$ [Fig. 1(b)].

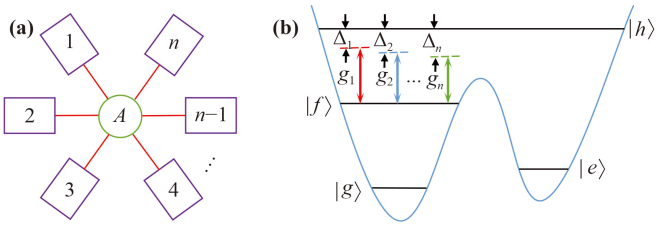

Fig. 1 **(a)** Schematic diagram of n microwave cavities coupled to a flux ququart. Each square represents a one-dimensional (1D) or three-dimensional (3D) cavity. The circle A in the middle represents the flux ququart, which is capacitively or inductively coupled to each cavity. **(b)** Cavity j $(j = 1,2,\cdots,n)$ is dispersively coupled to the $|f\rangle \leftrightarrow |h\rangle$ transition with coupling constant g_j and detuning Δ_j, while highly detuned (decoupled) from the transitions between any other two levels. It is noted that the transition between the two lowest levels $|g\rangle$ and $|e\rangle$ can be made weak by increasing the barrier between the two potential wells.

Under the dispersive-coupling condition $\Delta_j \gg g_j$ $(j = 1,2,\cdots,n)$, the energy exchange does not occur between the coupler ququart and the cavities. When the following condition meets

$$\frac{|\Delta_j - \Delta_k|}{|\Delta_j^{-1}| + |\Delta_k^{-1}|} \gg g_j g_k, \tag{4}$$

(where $j,k \in \{1,2,\cdots,n\}$, $j \neq k$), the interaction between any two of the cavities is not induced by the coupler ququart. Hence, under the dispersive couplings, one can obtain the following effective Hamiltonian [54–56]

$$H_{\mathrm{eff}} = -\sum_{j=1}^{n} \frac{g_j^2}{\Delta_j} \left(|f\rangle\langle f| a_j^+ a_j - |h\rangle\langle h| a_j a_j^+\right), \tag{5}$$

where the terms account for the ac-Stark shifts of the levels $|f\rangle$ and $|h\rangle$ of the ququart induced by the cavities. When the level $|h\rangle$ is not occupied, the Hamiltonian (5) reduces to

$$H_{\mathrm{eff}} = -\sum_{j=1}^{n} \lambda_j |f\rangle\langle f| a_j^+ a_j, \tag{6}$$

where $\lambda_j = g_j^2/\Delta_j$ $(j = 1,2,\cdots,n)$. As shown in the next section, this Hamiltonian (6) will be employed for the preparation of the entangled state (1) of multiple cat-state qutrits.

3 Generation of a maximally-entangled state of multiple cat-state qutrits

Let us return to the physical system depicted in

Fig. 1(a). The ququart is decoupled from the n cavities. Assume that the ququart is initially in the ground state $|g\rangle$ and each cavity is initially in a cat state $|\alpha\rangle+|-\alpha\rangle$. Note that this cat state has been experimentally created in circuit QED [34, 57–61]. The initial state of the whole system is thus given by

$$|\psi(0)\rangle = |g\rangle \otimes \prod_{j=1}^{n} (|\alpha\rangle_j + |-\alpha\rangle_j), \tag{7}$$

where subscript j represents cavity j ($j = 1, 2, \cdots, n$).

The entangled state preparation includes a few basic operations, described as follows:

Step (i): Apply resonant classical pulses (with appropriate frequencies, initial phases, and duration times) to the ququart. As shown in Appendix A, after the application of the pulses, one can obtain the following state transformation:

$$|g\rangle \to \frac{1}{\sqrt{3}}(|g\rangle + |e\rangle - |f\rangle). \tag{8}$$

The operation time required for achieving the state transformation (8) is given by $t_1 = (\arccos 1/\sqrt{3})/\Omega_{fg} + \pi/(4\Omega_{hf}) + \pi/(2\Omega_{he})$ (Appendix A). Thus, the state (7) becomes

$$|\psi\rangle_0 = \frac{1}{\sqrt{3}}(|g\rangle + |e\rangle - |f\rangle) \otimes \prod_{j=1}^{n} (|\alpha\rangle_j + |-\alpha\rangle_j). \tag{9}$$

Step (ii): Adjust the level spacings of the ququart such that the ququart is dispersively coupled to the cavities [Fig. 1(b)] to achieve an effective Hamiltonian (6). One can verify that under the Hamiltonian (6), the state (9) evolves as

$$\begin{aligned}|\psi\rangle_1 =& \frac{1}{\sqrt{3}}\Big[(|g\rangle + |e\rangle)\prod_{j=1}^{n}(|\alpha\rangle_j + |-\alpha\rangle_j) \\ &- |f\rangle\prod_{j=1}^{n}\left(|\alpha e^{i\lambda_j t_2}\rangle_j + |-\alpha e^{i\lambda_j t_2}\rangle_j\right)\Big],\end{aligned} \tag{10}$$

where t_2 is the ququart-cavity interaction time. By setting $\lambda_1 = \lambda_2 \cdots = \lambda_n = \lambda$ and choosing $t_2 = \pi/(3\lambda)$, the state (10) becomes

$$\begin{aligned}|\psi\rangle_2 =& \frac{1}{\sqrt{3}}\Big[(|g\rangle + |e\rangle)\prod_{j=1}^{n}(|\alpha\rangle_j + |-\alpha\rangle_j) \\ &- |f\rangle\prod_{j=1}^{n}\left(|\alpha e^{i\pi/3}\rangle_j + |-\alpha e^{i\pi/3}\rangle_j\right)\Big].\end{aligned} \tag{11}$$

After this step of operation, the level spacings of the ququart is adjusted such that the ququart is decoupled from the cavities.

Step (iii): Apply resonant classical pulses (with appropriate frequencies, initial phases, and duration times) to the ququart. As shown in Appendix B, after the application of the pulses, one can obtain the state transformation

$$|e\rangle \to |f\rangle,\ |f\rangle \to -|e\rangle. \tag{12}$$

The operation time required for achieving the state transformation (12) is given by $t_3 = \pi/\Omega_{he} + \pi/(2\Omega_{hf})$ (Appendix B). Hence, the state (11) changes to

$$\begin{aligned}|\psi\rangle_3 =& \frac{1}{\sqrt{3}}\Big[(|g\rangle + |f\rangle)\prod_{j=1}^{n}(|\alpha\rangle_j + |-\alpha\rangle_j) \\ &+ |e\rangle\prod_{j=1}^{n}\left(|\alpha e^{i\pi/3}\rangle_j + |-\alpha e^{i\pi/3}\rangle_j\right)\Big].\end{aligned} \tag{13}$$

Step (iv): Adjust the level spacings of the ququart such that the ququart is dispersively coupled to the cavities [Fig. 1(b)] to achieve an effective Hamiltonian (6). One can verify that under the Hamiltonian (6), the state (13) evolves as

$$\begin{aligned}|\psi\rangle_4 =& \frac{1}{\sqrt{3}}\Big[|g\rangle\prod_{j=1}^{n}(|\alpha\rangle_j + |-\alpha\rangle_j) + |f\rangle\prod_{j=1}^{n}\left(|\alpha e^{i\lambda_j t_4}\rangle_j\right. \\ &\left.+|-\alpha e^{i\lambda_j t_4}\rangle_j\right) + |e\rangle\prod_{j=1}^{n}\left(|\alpha e^{i\pi/3}\rangle_j + |-\alpha e^{i\pi/3}\rangle_j\right)\Big],\end{aligned} \tag{14}$$

where t_4 is the ququart-cavity interaction time. For $\lambda_1 = \lambda_2 \cdots = \lambda_n = \lambda$ (set above) and $t_4 = 2\pi/(3\lambda)$, the state (14) becomes

$$\begin{aligned}|\psi\rangle_5 =& \frac{1}{\sqrt{3}}\Big[|g\rangle\prod_{j=1}^{n}(|\alpha\rangle_j + |-\alpha\rangle_j) + |f\rangle\prod_{j=1}^{n}\left(|\alpha e^{i2\pi/3}\rangle_j\right. \\ &\left.+|-\alpha e^{i2\pi/3}\rangle_j\right) + |e\rangle\prod_{j=1}^{n}\left(|\alpha e^{i\pi/3}\rangle_j + |-\alpha e^{i\pi/3}\rangle_j\right)\Big].\end{aligned} \tag{15}$$

After this step of operation, the level spacings of the ququart is adjusted such that the ququart is decoupled from the cavities. Note that the cat states above have the same normalized constant. Hence, the normalized constant is omitted in the above equations for simplicity.

After having the state (15) normalized and in terms of Eq. (2), the state (15) can be rewritten as

$$|\psi\rangle_6 = \frac{1}{\sqrt{3}}\left(|g\rangle\prod_{j=1}^{n}|C_0\rangle_j + |f\rangle\prod_{j=1}^{n}|C_2\rangle_j + |e\rangle\prod_{j=1}^{n}|C_1\rangle_j\right). \tag{16}$$

Eq. (15) or Eq. (16) shows that the ququart is entangled with the cavities. The purpose of the remaining step of operation is to disentangle the ququart from the cavities.

Step (v): Apply resonant classical pulses (with appropriate frequencies, initial phases, and duration times) to

the ququart. As shown in Appendix C, after the application of the pulses, one can obtain the following state transformation

$$\begin{aligned}
|g\rangle &\to \frac{1}{\sqrt{3}}\left(|g\rangle+|e\rangle+|f\rangle\right),\\
|e\rangle &\to \frac{1}{\sqrt{3}}\left(|g\rangle+\omega|e\rangle+\omega^2|f\rangle\right),\\
|f\rangle &\to \frac{1}{\sqrt{3}}\left(|g\rangle+\omega^2|e\rangle+\omega|f\rangle\right),
\end{aligned} \tag{17}$$

where $\omega=\mathrm{e}^{\mathrm{i}2\pi/3}$. The operation time required for achieving the state transformation (17) is given by $t_5=\pi/\left(2\Omega_{hf}\right)+\pi/\left(2\Omega_{fg}\right)+\pi/\Omega_{he}+\arccos\sqrt{2/3}/\Omega_{fg}$ (Appendix C). According to Eq. (17), the state (16) changes to

$$\begin{aligned}
|\psi\rangle_7 =&\frac{1}{\sqrt{3}}\left(\prod_{j=1}^{n}|C_0\rangle_j+\prod_{j=1}^{n}|C_1\rangle_j+\prod_{j=1}^{n}|C_2\rangle_j\right)|g\rangle\\
&+\frac{1}{\sqrt{3}}\left(\prod_{j=1}^{n}|C_0\rangle_j+\omega\prod_{j=1}^{n}|C_1\rangle_j+\omega^2\prod_{j=1}^{n}|C_2\rangle_j\right)|e\rangle\\
&+\frac{1}{\sqrt{3}}\left(\prod_{j=1}^{n}|C_0\rangle_j+\omega^2\prod_{j=1}^{n}|C_1\rangle_j+\omega\prod_{j=1}^{n}|C_2\rangle_j\right)|f\rangle.
\end{aligned} \tag{18}$$

Eq. (18) implies that if the ququart is detected in the state $|g\rangle$, $|e\rangle$, or $|f\rangle$, the n cavities will be respectively in the following entangled states:

$$\begin{aligned}
|\mathrm{ENT}\rangle_1 &= \frac{1}{\sqrt{3}}\left(\prod_{j=1}^{n}|C_0\rangle_j+\prod_{j=1}^{n}|C_1\rangle_j+\prod_{j=1}^{n}|C_2\rangle_j\right),\\
|\mathrm{ENT}\rangle_2 &= \frac{1}{\sqrt{3}}\left(\prod_{j=1}^{n}|C_0\rangle_j+\omega\prod_{j=1}^{n}|C_1\rangle_j+\omega^2\prod_{j=1}^{n}|C_2\rangle_j\right),\\
|\mathrm{ENT}\rangle_3 &= \frac{1}{\sqrt{3}}\left(\prod_{j=1}^{n}|C_0\rangle_j+\omega^2\prod_{j=1}^{n}|C_1\rangle_j+\omega\prod_{j=1}^{n}|C_2\rangle_j\right).
\end{aligned} \tag{19}$$

One can see that the three states given in Eq. (19) are also the entangled states of the n cat-state qutrits $(1,2,\cdots,n)$, for each of them the three logic states are encoded via the three cat states $|C_0\rangle$, $|C_1\rangle$, and $|C_2\rangle$. In the introduction, we have mentioned that for a sufficiently large α, any two of the three cat states are quasi-orthogonal to each other. Therefore, when α is large enough, the states given in Eq. (19) are the maximally-entangled states of the n cat-state qutrits to a very good approximation.

From the above description, one can easily see that:

(i) The higher-energy level $|h\rangle$ of the ququart is occupied only in steps (i), (iii), and (v). Since these steps only employ the ququart-pulse resonant interactions and thus can be fast completed within a short time, the higher-energy level $|h\rangle$ of the ququart is occupied only for a short time during the entire state preparation. Thus, decoherence from this level is greatly suppressed.

(ii) The total operation time for the entangled state preparation is given by

$$t_{\mathrm{op}}=\tau_1+\tau_2, \tag{20}$$

where

$$\begin{aligned}
\tau_1 =& 5\pi/\left(4\Omega_{hf}\right)+5\pi/\left(2\Omega_{he}\right)\\
&+\left(\pi/2+\arccos 1/\sqrt{3}+\arccos\sqrt{2/3}\right)/\Omega_{fg}+4\tau_d,
\end{aligned} \tag{21}$$

$$\tau_2=\pi/\lambda. \tag{22}$$

Here, τ_1 is the total of operational time for steps (i), (iii), and (v), while τ_2 is the total of operational time for steps (ii) and (iv). Note that τ_d is the typical time required for adjusting the level spacings of the ququart, which is about 1–3 ns [52, 53]. From Eqs. (20)–(22), one can see that the entire operation time for the entangled state preparation is independent of the number of the qutrits (n) involved in the entangled state. Thus, the operation time does not increase with the number of the qutrits.

(iii) The above condition $\lambda_1=\lambda_2\cdots=\lambda_n$ turns out to be

$$\frac{g_1^2}{\Delta_1}=\frac{g_2^2}{\Delta_2}=\cdots=\frac{g_n^2}{\Delta_n}, \tag{23}$$

which can be easily established by carefully selecting Δ_j through appropriately choosing the frequency ω_{c_j} of cavity j due to $\Delta_j=\omega_{fg}-\omega_{c_j}$ $(j=1,2,\cdots,n)$. In addition, the condition (23) can be achieved by varying g_j, e.g., through adjusting the capacitance c_j between cavity j and the ququart.

(iv) During the entangled state preparation, the ququart is coupled or decoupled to the cavities by adjusting the ququart's level spacings. Alternatively, the ququart can be made to be coupled or decoupled to the cavities by adjusting the frequency of each cavity. For a superconducting microwave cavity, its frequency can be quickly (within a few nanoseconds) tuned in experiments [62, 63].

(v) The entangled states (19) are produced depending on the outcome of the measurement on the ququart. It should be mentioned that experiments have reported rapid and accurate measurement of the states of superconducting artificial atoms [64, 65].

(vi) This protocol is also suitable for the case of coherent states. The three logic states of each qutrit can be coherent states. For instance, they can be: $|C_0'\rangle=|\alpha\rangle$, $|C_1'\rangle=|\alpha\mathrm{e}^{\mathrm{i}\pi/3}\rangle$, and $|C_2'\rangle=|\alpha\mathrm{e}^{\mathrm{i}2\pi/3}\rangle$. In this case, the procedure for preparing the entangled state (1), with the three cat states replaced by the three coherent states here, is the same as the preparation process described above.

(vii) In the above, we have assumed that all detunings

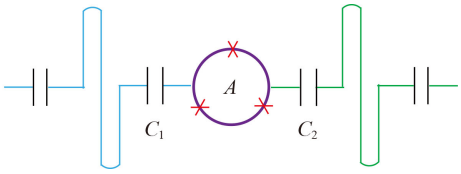

Fig. 2 Setup for two 1D microwave cavities and a SC flux ququart (the circle A in the middle). Each cavity is a transmission line resonator. The flux ququart consists of three Josephson junctions and a superconducting loop, which is linked to each cavity via a capacitor.

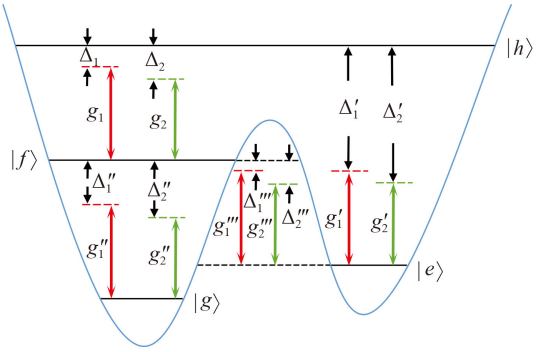

Fig. 3 Illustration of the unwanted coupling between cavity j $(j=1,2)$ and the $|e\rangle \leftrightarrow |h\rangle$ transition with coupling constant g_j' and detuning Δ_j'. Illustration of cavity j $(j=1,2)$ and the $|g\rangle \leftrightarrow |f\rangle$ transition with coupling constant g_j'' and detuning Δ_j''. Illustration of cavity j $(j=1,2)$ and the $|e\rangle \leftrightarrow |f\rangle$ transition with coupling constant g_j''' and detuning Δ_j'''. Red lines correspond to cavity 1, while green lines correspond to cavity 2.

are positive. However, it is worth noting that the protocol also applies to the negative detunings.

Before ending this section, it should be mentioned that our proposal presented above does not consider the inter-cavity crosstalk. As shown above, when the inter-cavity crosstalk is not taken into account, this proposal can *in principle* be used to create the entangled states (19) of multiple cat-state qutrits. In reality, there is an unwanted inter-cavity crosstalk during the entangled state preparation. As demonstrated in the following subsection D, the scalability of this proposal, i.e., the fidelity of the entangled states (19) with multiple cat-state qutrits, is limited by the inter-cavity crosstalk. To make our proposal have a good scalability, one would need to reduce the inter-cavity crosstalk in experiments, especially when a number of cavities are involved.

4 Experimental feasibility

As an example, we investigate the experimental feasibility for preparing the maximally-entangled state of two cat-state qutrits, by employing a setup of two 1D microwave cavities or resonators coupled to a flux ququart (Fig. 2). As mentioned previously, because steps (i), (iii), and (v) only employ the ququart-pulse resonant interactions, the operations in these steps can be fast completed within a very short time (e.g., by increasing the pulse Rabi frequencies). Thus, for steps (i), (iii), and (v), the effect of the ququart decoherence, the cavity dissipation, and the inter-cavity crosstalk is negligibly small. In this sense, the effect of the system dissipation and the inter-cavity crosstalk would appear in steps (ii) and (iv) because these two steps require a relatively long operation time due to the use of the ququart-cavity dispersive interaction [Fig. 1(b)].

4.1 Full Hamiltonian

After considering the unwanted couplings between the cavities and the ququart's level transitions (see Fig. 3) as well as the inter-cavity crosstalk, the Hamiltonian H_I in Eq. (3), with $n=2$ for the present case, is modified as

$$H_I' = \sum_{j=1}^{2} g_j \left(e^{i\Delta_j t} a_j |h\rangle\langle f| + \text{h.c.}\right) + \sum_{j=1}^{2} g_j' \left(e^{i\Delta_j' t} a_j |h\rangle\langle e| + \text{h.c.}\right) + \sum_{j=1}^{2} g_j'' \left(e^{i\Delta_j'' t} a_j |f\rangle\langle g| + \text{h.c.}\right) + \sum_{j=1}^{2} g_j''' \left(e^{i\Delta_j''' t} a_j |f\rangle\langle e| + \text{h.c.}\right) + \varepsilon, \tag{24}$$

where the second term represents the unwanted coupling between cavity j and the $|e\rangle \leftrightarrow |h\rangle$ transition with coupling constant g_j' and detuning $\Delta_j' = \omega_{he} - \omega_{c_j}$ $(j=1,2)$, the third term represents the unwanted coupling between cavity j and the $|g\rangle \leftrightarrow |f\rangle$ transition with coupling constant g_j'' and detuning $\Delta_j'' = \omega_{fg} - \omega_{c_j}$ $(j=1,2)$, and the fourth term represents the unwanted coupling between cavity j and the $|e\rangle \leftrightarrow |f\rangle$ transition with coupling constant g_j''' and detuning $\Delta_j''' = \omega_{fe} - \omega_{c_j}$ $(j=1,2)$ (Fig. 3). Here, ω_{he}, ω_{fg}, and ω_{fe} are the $|e\rangle \leftrightarrow |h\rangle$ transition frequency, the $|g\rangle \leftrightarrow |f\rangle$ transition frequency, and the $|e\rangle \leftrightarrow |f\rangle$ transition frequency of the ququart, respectively. In Eq. (24), ε is the Hamiltonian characterizing the inter-cavity crosstalk, given by

$$\varepsilon = g_{12} e^{i\Delta_{12} t} a_1^{+} a_2 + \text{h.c.}, \tag{25}$$

where g_{12} is the crosstalk strength between the two cavities, and $\Delta_{12} = \omega_{c_1} - \omega_{c_2}$ is the frequency difference between the two cavities. Note that the couplings of each cavity with the $|g\rangle \leftrightarrow |h\rangle$ and $|g\rangle \leftrightarrow |e\rangle$ transitions are negligible because each cavity is highly detuned from the $|g\rangle \leftrightarrow |h\rangle$ transition (i.e., $\omega_{hg} \gg \omega_{c_j}$, $j=1,2$) and the $|g\rangle \leftrightarrow |e\rangle$ transition is weak due to the barrier between the two potential wells. Therefore, these unwanted couplings are not considered in the Hamiltonian (24) to simplify the numerical simulations.

Table 1 Parameters used in the numerical simulation. For the definitions of the parameters, please refer to the text.

$\omega_{eg}/(2\pi) = 3\,\text{GHz}$	$\omega_{fg}/(2\pi) = 11\,\text{GHz}$	$\omega_{he}/(2\pi) = 17\,\text{GHz}$
$\omega_{hf}/(2\pi) = 9\,\text{GHz}$	$\omega_{hg}/(2\pi) = 20\,\text{GHz}$	$\omega_{c_1}/(2\pi) = 7.5\,\text{GHz}$
$\omega_{c_2}/(2\pi) = 6.5\,\text{GHz}$	$\triangle_1/(2\pi) = 1.5\,\text{GHz}$	$\triangle_1'/(2\pi) = 9.5\,\text{GHz}$
$\triangle_1''/(2\pi) = 3.5\,\text{GHz}$	$\triangle_1'''/(2\pi) = 0.5\,\text{GHz}$	$\triangle_2/(2\pi) = 2.5\,\text{GHz}$
$\triangle_2'/(2\pi) = 10.5\,\text{GHz}$	$\triangle_2''/(2\pi) = 4.5\,\text{GHz}$	$\triangle_2'''/(2\pi) = 1.5\,\text{GHz}$
$\triangle_{12}/(2\pi) = 1.0\,\text{GHz}$	$g_1/(2\pi) = 75\,\text{MHz}$	$g_1'/(2\pi) = 75\,\text{MHz}$
$g_1''/(2\pi) = 53.04\,\text{MHz}$	$g_1'''/(2\pi) = 7.5\,\text{MHz}$	$g_2/(2\pi) = 96.82\,\text{MHz}$
$g_2'/(2\pi) = 96.82\,\text{MHz}$	$g_2''/(2\pi) = 68.47\,\text{MHz}$	$g_2'''/(2\pi) = 9.682\,\text{MHz}$

4.2 Numerical results

During the operation of step (ii) or step (iv), the dynamics of the lossy system is determined by the following master equation

$$\begin{aligned}\frac{\mathrm{d}\rho}{\mathrm{d}t} =& -\mathrm{i}\,[H_I', \rho] + \sum_{j=1}^{2} \kappa_j \mathcal{L}\,[a_j] \\ &+ \gamma_{eg}\mathcal{L}\left[\sigma_{eg}^{-}\right] + \gamma_{fe}\mathcal{L}\left[\sigma_{fe}^{-}\right] + \gamma_{fg}\mathcal{L}\left[\sigma_{fg}^{-}\right] \\ &+ \gamma_{hf}\mathcal{L}\left[\sigma_{hf}^{-}\right] + \gamma_{he}\mathcal{L}\left[\sigma_{he}^{-}\right] + \gamma_{hg}\mathcal{L}\left[\sigma_{hg}^{-}\right] \\ &+ \sum_{s} \gamma_{s,\varphi}\left(\sigma_{ss}\rho\sigma_{ss} - \sigma_{ss}\rho/2 - \rho\sigma_{ss}/2\right), \end{aligned} \tag{26}$$

where $\mathcal{L}\,[\Lambda] = \Lambda\rho\Lambda^{+} - \Lambda^{+}\Lambda\rho/2 - \rho\Lambda^{+}\Lambda/2$ (with $\Lambda = a_j, \sigma_{eg}^{-}, \sigma_{fe}^{-}, \sigma_{fg}^{-}, \sigma_{hf}^{-}, \sigma_{he}^{-}, \sigma_{hg}^{-}$), $\sigma_{eg}^{-} = |g\rangle\langle e|$, $\sigma_{fe}^{-} = |e\rangle\langle f|$, $\sigma_{fg}^{-} = |g\rangle\langle f|$, $\sigma_{hf}^{-} = |f\rangle\langle h|$, $\sigma_{he}^{-} = |e\rangle\langle h|$, $\sigma_{hg}^{-} = |g\rangle\langle h|$, $\sigma_{ss} = |s\rangle\langle s|$ $(s = h, f, e)$. In addition, κ_j is the decay rate of cavity j $(j = 1, 2)$, γ_{eg} is the energy relaxation rate for the level $|e\rangle$ of the ququart associated with the decay path $|e\rangle \to |g\rangle$; γ_{fe} and γ_{fg} are the relaxation rates for the level $|f\rangle$ of the ququart related to the decay paths $|f\rangle \to |e\rangle$ and $|f\rangle \to |g\rangle$, respectively; γ_{hf}, γ_{he}, and γ_{hg} are, respectively, the relaxation rates for the level $|f\rangle$ of the ququart related to the decay paths $|h\rangle \to |f\rangle$, $|h\rangle \to |e\rangle$, and $|h\rangle \to |g\rangle$; $\gamma_{e,\varphi}$, $\gamma_{f,\varphi}$, and $\gamma_{h,\varphi}$ are, respectively, the dephasing rates of the levels $|e\rangle$, $|f\rangle$, and $|h\rangle$ of the ququart.

The fidelity of the entire operation is estimated by

$$\mathcal{F} = \sqrt{\langle\psi_{id}|\rho|\psi_{id}\rangle}, \tag{27}$$

where $|\psi_{id}\rangle$ is the ideal output state given by Eq. (15) for $n = 2$, while ρ is the final density matrix of the whole system obtained by numerically solving the master equation. For numerical calculations, we here use the QUTIP software [66, 67], which is open-source software for simulating the dynamics of open quantum systems.

Table 1 provides the parameters used in the numerical simulations. The coupling constant g_2 is calculated by using Eq. (23). The $|g\rangle \leftrightarrow |e\rangle$ and $|e\rangle \leftrightarrow |f\rangle$ transitions are much weaker due to the barrier between the two potential wells. Define ϕ_{ij} as the dipole coupling matrix element between the two levels $|i\rangle$ and $|j\rangle$ with $ij \in \{he, hf, fg, fe, eg\}$. One can have $\phi_{hg} \sim \phi_{he} \sim \phi_{hf} \sim \sqrt{2}\phi_{fg} \sim 10\phi_{fe} \sim 50\phi_{eg}$ through properly designing the flux ququart [68, 69]. In this sense, one has $g_j' \sim g_j$, $g_j'' \sim g_j/\sqrt{2}$, $g_j''' \sim 0.1g_j$ $(j = 1, 2)$. Among the coupling constants listed in Table 1, the maximum is $g_{\max} = 2\pi \times 96.82$ MHz, which is readily achievable since a coupling constant ranging from $2\pi \times 636$ MHz to $2\pi \times 7.27$ GHz has been reported in experiments for a flux device coupled to a microwave cavity [70–72].

Other parameters employed in the numerical simulations are: (i) $\gamma_{eg}^{-1} = 100$ μs, $\gamma_{fe}^{-1} = 50$ μs, $\gamma_{hg}^{-1} = \gamma_{he}^{-1} = \gamma_{hf}^{-1} = \gamma_{fg}^{-1}/2 = 10$ μs, $\gamma_{h,\varphi}^{-1} = \gamma_{f,\varphi}^{-1} = \gamma_{e,\varphi}^{-1} = 5$ μs, (ii) $\kappa_1 = \kappa_2 = \kappa$, and (iii) $\alpha = 2.2$. Here, γ_{eg}^{-1} and γ_{fe}^{-1} are much greater than $\{\gamma_{hg}^{-1}, \gamma_{he}^{-1}, \gamma_{hf}^{-1}, \gamma_{fg}^{-1}\}$ because of $\phi_{eg}, \phi_{fe} \ll \{\phi_{hg}, \phi_{he}, \phi_{hf}, \phi_{fg}\}$ due to the barrier between the two potential wells. We choose $\gamma_{hg}^{-1} = \gamma_{he}^{-1} = \gamma_{hf}^{-1} = \gamma_{fg}^{-1}/2$ because of $\phi_{hg} \sim \phi_{he} \sim \phi_{hf} \sim \sqrt{2}\phi_{fg}$. In addition, we choose $\gamma_{h,\varphi}^{-1} = \gamma_{f,\varphi}^{-1} = \gamma_{e,\varphi}^{-1}$ because the dephasing times for the three excited levels $|e\rangle$, $|f\rangle$, and $|h\rangle$ are not related to the dipole matrix elements and are on the same order. The decoherence times with the values given here are a conservative case because experiments have reported decoherence time 70 μs to 1 ms for a superconducting flux device [47, 73, 74].

By numerically solving the master equation (26), we plot Fig. 4 which shows the fidelity versus κ^{-1} for $g_{12} = 0$, $0.01g_{\max}$, and $0.05g_{\max}$. From Fig. 4, one can see that the fidelity exceeds 95.44% for $\kappa^{-1} \geq 50$ μs and $g_{12} = 0.05g_{\max}$. The setting $g_{12} \leq 0.05g_{\max}$ can be obtained experimentally by a prior design of the sample with appropriate capacitances C_1 and C_2 shown in Fig. 2 [75].

4.3 Discussion

The infidelity is mainly caused due to the system dissipation, the unwanted ququart-cavity interaction, and the validity of the effective Hamiltonian (5). The fidelity can be further improved by: (i) select the ququart with larger level spacing anharmonicity and longer decoherence time, (ii) choose the cavities with a high quality factor, and (iii) optimize the ratio Δ_j/g_j to better meet the large detuning condition for the effective Hamiltonian.

As mentioned above, to simplify the numerical simula-

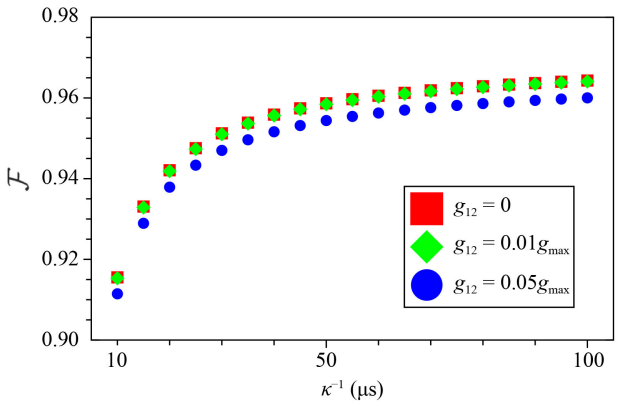

Fig. 4 Fidelity versus κ^{-1} for $g_{12}/g_{\max} = 0, 0.01, 0.05$. Here, κ is the cavity decay rate, and g_{12} is the inter-cavity crosstalk strength between cavities 1 and 2. The parameters used in the numerical simulation are referred to the text and Table 1.

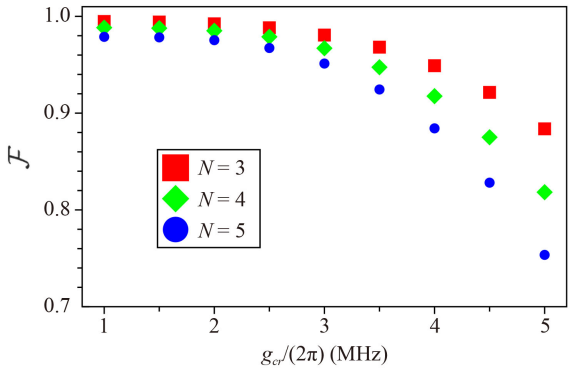

Fig. 5 Fidelity versus g_{cr} for three cavities ($n = 3$), four cavities ($n = 4$), and five cavities ($n = 5$). Here, assume that the crosstalk strength g_{cr} between any two cavities is identical. The system dissipation and the unwanted cavity-ququart couplings are not considered in the numerical simulation.

tions, we did not consider: (i) The coupling of each cavity with the $|g\rangle \leftrightarrow |h\rangle$ and $|g\rangle \leftrightarrow |e\rangle$ transitions, (ii) The system dissipation and the inter-cavity crosstalk during the adjustment of the ququart level spacings, and (iii) The system dissipation and the inter-cavity crosstalk in steps (i), (iii), and (v). However, when they are taken into account, the fidelity would be slightly decreased. Reasons for this are as follows. First, as stated above, the couplings of each cavity with the $|g\rangle \leftrightarrow |h\rangle$ and $|g\rangle \leftrightarrow |e\rangle$ transitions are negligible because of $\omega_{hg} \gg \omega_{c_j}$ and the weak $|g\rangle \leftrightarrow |e\rangle$ transition (Fig. 2). Second, the system dissipation and the inter-cavity crosstalk can be neglected during rapidly adjusting the ququart level spacings [52, 53]. Last, as already explained above, they are negligibly small in steps (i), (iii), and (v). Finally, it should be mentioned that the fidelity was calculated without considering the measurement errors, which however could be negligible because fast and highly accurate measurements on the states of superconducting artificial atoms have been experimentally reported [64, 65].

Consider $\Omega_{hf} = \Omega_{he} = \Omega_{fg} = 2\pi \times 100$ MHz (available in experiments [76]). In addition, assume $\tau_d = 1$ ns. The total of operational time for steps (i), (iii), and (v) is $\tau_1 \sim 0.027$ μs, which is calculated based on Eq. (21). For the parameters Δ_j and g_j given in Table 1 ($j = 1, 2$), a simple calculation gives $\lambda = g_j^2/\Delta_j \sim 2\pi \times 3.75$ MHz. Thus, according to Eq. (22), the total operational time for steps (ii) and (iv) is estimated as $\tau_2 \sim 0.133$ μs. For the values of τ_1 and τ_2 here, it is obvious to have $\tau_1 \ll \tau_2$. The entire operational time for the entangled state preparation is $\tau_1 + \tau_2 \sim 0.16$ μs, which is much shorter than decoherence times of the ququart used in the numerical calculations and the cavity decay times (10–100 μs) considered in Fig. 4. Finally, with the cavity frequencies in Table 1 and $\kappa^{-1} = 50$ μs, the quality factors of the two cavities are $Q_1 \sim 2.35 \times 10^6$ and $Q_2 \sim 2.04 \times 10^6$, which are available because a 1D microwave cavity with a high quality factor $Q \gtrsim 2.7 \times 10^6$ was reported in experiments [77, 78].

The above analysis implies that high-fidelity generation of the maximally-entangled state of two cat-state qutrits is feasible with current circuit QED experiments. We remark that further investigation is needed for each specific experimental setup. However, this requires a rather lengthy and complex analysis, which is beyond the scope of this theoretical work.

4.4 Scalability of this proposal

To further investigate the effects of the inter-cavity crosstalk on the scalability of this proposal, let us take three cavities, four cavities, and five cavities as examples, i.e., consider $n = 3$, 4, 5. We choose $\Delta_1/(2\pi) = 1.5$ GHz and use the relation $\Delta_j/(2\pi) = \Delta_{j-1}/(2\pi) + 1$ GHz for the detunings [Fig. 1(b)], with $j = 2, 3, \cdots, n$. In addition, we choose $g_1/(2\pi) = 30$ MHz. According to Eq. (23), the coupling constant g_j between cavity j and the ququart is set as $g_j = \sqrt{\Delta_j/\Delta_1}\, g_1$ ($j = 2, 3, \cdots, n$). For simplicity, we assume that the crosstalk strength g_{cr} between any two cavities is identical.

We numerically plot Fig. 5 which shows the fidelity versus g_{cr}. To highlight the effect of the inter-cavity crosstalk, Fig. 5 is plotted without considering the system dissipation and the cavity-ququart unwanted couplings. Figure 5 shows that for $g_{cr}/(2\pi) \leq 2$ MHz, the fidelity exceeds 99.2%, 98.5%, and 97.5% for $n = 3$ (three cavities), $n = 4$ (four cavities), and $n = 5$ (five cavities), respectively.

Figure 5 reveals that for a given g_{cr}, the fidelity decreases as the number of cavities increases. Moreover, Fig. 5 shows that for a larger g_{cr}, the fidelity drops faster with the increasing number of cavities. These results imply that the fidelity of the entangled states (19)

is sensitive to the inter-cavity crosstalk, and this influence becomes more pronounced when the number of cavities increases. Therefore, in order to achieve a good scalability of this proposal, that is, to obtain high fidelity of the entangled states (19) with multiple cat-state qutrits (involving multiple cavities), the inter-cavity crosstalk will need to be reduced in experiments.

5 Conclusion

We have proposed an efficient method to prepare a maximally-entangled state of multiple cat-state qutrits in circuit QED. The entangled state is created by using multiple microwave cavities coupled to a superconducting ququart. Because of utilizing only a coupler ququart, the circuit hardware resource is greatly reduced. Since the higher intermediate level of the ququart is occupied only for a short time, decoherence from this level is significantly suppressed during the state preparation. More interestingly, the operational time for the entangled state preparation does not depend on the number of the qutrits, therefore it does not increase with the number of the qutrits. Our numerical simulations show that, with the current circuit QED technology, the high-fidelity preparation is feasible for a maximally entangled state of two cat-state qutrits. We have also numerically analyzed the effect of the inter-cavity crosstalk on the scalability of this proposal. This proposal is generic and can be extended to accomplish the same task by employing multiple microwave or optical cavities coupled to a natural or artificial four-level atom. Finally, this proposal can be applied to create a maximally-entangled state with qutrits encoded via coherent states. We hope that this work will stimulate experimental activities in the near future.

Declarations The authors declare that they have no competing interests and there are no conflicts.

Acknowledgements This work was partly supported by the National Natural Science Foundation of China (NSFC) (Grant Nos. 11074062, 11374083, 11774076, and U21A20436), the Key-Area Research and Development Program of Guangdong Province (No. 2018B030326001), the Jiangsu Funding Program for Excellent Postdoctoral Talent, and the Innovation Program for Quantum Science and Technology (No. 2021ZD0301705).

Appendix

In this appendix, we first introduce several ququart-pulse resonant interactions and the state evolutions under these resonant interactions, we then explicitly show how to implement the state transformations (8,12, 17) given in the main text, by applying resonant classical pulses to the ququart.

The first resonant interaction is: A classical pulse is resonant with the $|g\rangle \leftrightarrow |f\rangle$ transition of the ququart. In the interaction picture, the Hamiltonian describing this resonant interaction is given by

$$H_1 = \Omega_{fg} e^{i\phi} |g\rangle\langle f| + \text{H.c.}, \tag{A1}$$

where ϕ is the initial phase of the pulse while Ω_{fg} is the Rabi frequency of the pulse. From this Hamiltonian, it is straightforward to see that a pulse of duration t results in the following state rotation:

$$\begin{aligned} |g\rangle &\to \cos\Omega_{fg}t|g\rangle - ie^{-i\phi}\sin\Omega_{fg}t|f\rangle, \\ |f\rangle &\to -ie^{i\phi}\sin\Omega_{fg}t|g\rangle + \cos\Omega_{fg}t|f\rangle. \end{aligned} \tag{A2}$$

The second resonant interaction is: A classical pulse is resonant with the $|f\rangle \leftrightarrow |h\rangle$ transition of the ququart. In the interaction picture, the Hamiltonian is given by

$$H_2 = \Omega_{hf} e^{i\phi} |f\rangle\langle h| + \text{H.c.}, \tag{A3}$$

where Ω_{hf} is the Rabi frequency of the pulse. From this Hamiltonian, it is easy to see that a pulse of duration t results in the following state rotation:

$$\begin{aligned} |f\rangle &\to \cos\Omega_{hf}t|f\rangle - ie^{-i\phi}\sin\Omega_{hf}t|h\rangle, \\ |h\rangle &\to -ie^{i\phi}\sin\Omega_{hf}t|f\rangle + \cos\Omega_{hf}t|h\rangle. \end{aligned} \tag{A4}$$

The last resonant interaction is: A classical pulse is resonant with the $|e\rangle \leftrightarrow |h\rangle$ transition of the ququart. In the interaction picture, the Hamiltonian characterizing this resonant interaction is given by

$$H_3 = \Omega_{he} e^{i\phi} |e\rangle\langle h| + \text{H.c.}, \tag{A5}$$

where Ω_{he} is the Rabi frequency of the pulse. Based on this Hamiltonian, one can easily find that a pulse of duration t leads to the following state rotation:

$$\begin{aligned} |e\rangle &\to \cos\Omega_{he}t|e\rangle - ie^{-i\phi}\sin\Omega_{he}t|h\rangle, \\ |h\rangle &\to -ie^{i\phi}\sin\Omega_{he}t|e\rangle + \cos\Omega_{he}t|h\rangle. \end{aligned} \tag{A6}$$

As shown below, the state evolutions (A2, A4, A6) obtained above will be used to implement the state transformations (8, 12, 17) in the main text.

Appendix A: Implementing the state transformation (8)

The state transformation (8) is implemented through the following three basic operations:

(i) Apply a classical pulse (with $\phi = \pi/2$) to the ququart. The pulse is resonant with the $|g\rangle \leftrightarrow |f\rangle$ transition. After the pulse duration $\left(\arccos 1/\sqrt{3}\right)/\Omega_{fg}$, the transformation $|g\rangle \to \frac{1}{\sqrt{3}}|g\rangle - \sqrt{\frac{2}{3}}|f\rangle$ is obtained according to Eq. (A2).

(ii) Apply a classical pulse (with $\phi = \pi/2$) to the ququart. The pulse is resonant with the $|f\rangle \leftrightarrow |h\rangle$ transition. After the pulse duration $\pi/(4\Omega_{hf})$, the transformation

$|f\rangle \to \frac{1}{\sqrt{2}}(|f\rangle - |h\rangle)$ is realized according to Eq. (A4); while the state $|g\rangle$ remains unchanged.

(iii) Apply a classical pulse (with $\phi = \pi/2$) to the ququart. The pulse is resonant with the $|e\rangle \leftrightarrow |h\rangle$ transition. After the pulse duration $\pi/(2\Omega_{he})$, the transformation $|h\rangle \to |e\rangle$ is achieved according to Eq. (A6); while the states $|g\rangle$ and $|f\rangle$ remain unchanged.

The states of the ququart after each basic operation are summarized below:

$$\begin{aligned} |g\rangle &\xrightarrow{\text{(i)}} \frac{1}{\sqrt{3}}|g\rangle - \sqrt{\frac{2}{3}}|f\rangle \\ &\xrightarrow{\text{(ii)}} \frac{1}{\sqrt{3}}(|g\rangle - |f\rangle + |h\rangle) \\ &\xrightarrow{\text{(iii)}} \frac{1}{\sqrt{3}}(|g\rangle + |e\rangle - |f\rangle), \end{aligned} \tag{A7}$$

which shows that the state transformation (8) in the main text is implemented after the above three basic operations. From the descriptions given above, one can see that the operation time required for implementing the state transformation (8) is $t_1 = (\arccos 1/\sqrt{3})/\Omega_{fg} + \pi/(4\Omega_{hf}) + \pi/(2\Omega_{he})$.

Appendix B: Implementing the state transformation (12)

The state transformation (12) is implemented using the following three basic operations:

(i) Apply a classical pulse (with $\phi = -\pi/2$) to the ququart. The pulse is resonant with the $|e\rangle \leftrightarrow |h\rangle$ transition. After the pulse duration $\pi/(2\Omega_{he})$, the transformation $|e\rangle \to |h\rangle$ is obtained according to Eq. (A6); while the state $|f\rangle$ remains unchanged.

(ii) Apply a classical pulse (with $\phi = \pi/2$) to the ququart. The pulse is resonant with the $|f\rangle \leftrightarrow |h\rangle$ transition. After the pulse duration $\pi/(2\Omega_{hf})$, the transformation $|f\rangle \to -|h\rangle$ and $|h\rangle \to |f\rangle$ is achieved according to Eq. (A4).

(iii) Apply a classical pulse (with $\phi = \pi/2$) to the ququart. The pulse is resonant with the $|e\rangle \leftrightarrow |h\rangle$ transition. After the pulse duration $\pi/(2\Omega_{he})$, the transformation $|h\rangle \to |e\rangle$ is realized according to Eq. (A6); while the state $|f\rangle$ remains unchanged.

The states of the ququart after each basic operation are summarized below:

$$\begin{aligned} &|e\rangle \xrightarrow{\text{(i)}} |h\rangle \xrightarrow{\text{(ii)}} |f\rangle \xrightarrow{\text{(iii)}} |f\rangle, \\ &|f\rangle \xrightarrow{\text{(i)}} |f\rangle \xrightarrow{\text{(ii)}} -|h\rangle \xrightarrow{\text{(iii)}} -|e\rangle, \end{aligned} \tag{A8}$$

which shows that the state transformation (12) in the main text is realized after the above three basic operations. Based on the descriptions presented above, one can see that the operation time required for implementing the state transformation (12) is $t_3 = \pi/\Omega_{he} + \pi/(2\Omega_{hf})$.

Appendix C: Realizing the state transformation (17)

The state transformation (17) is implemented through the following basic operations:

(i) Apply a classical pulse (with $\phi = -\pi/2$) to the ququart. The pulse is resonant with the $|e\rangle \leftrightarrow |h\rangle$ transition. After the pulse duration $\pi/(2\Omega_{he})$, one obtains the transformation $|e\rangle \to |h\rangle$ according to Eq. (A6); while the states $|g\rangle$ and $|f\rangle$ remain unchanged.

(ii) Apply a classical pulse (with $\phi = \pi/2$) to the ququart. The pulse is resonant with the $|f\rangle \leftrightarrow |h\rangle$ transition. After the pulse duration $\pi/(4\Omega_{hf})$, one obtains the transformation $|f\rangle \to \frac{1}{\sqrt{2}}(|f\rangle - |h\rangle)$ and $|h\rangle \to \frac{1}{\sqrt{2}}(|f\rangle + |h\rangle)$ according to Eq. (A4); while the state $|g\rangle$ remains unchanged.

(iii) Apply a classical pulse (with $\phi = 0$) to the ququart. The pulse is resonant with the $|g\rangle \leftrightarrow |f\rangle$ transition. After the pulse duration $\pi/(2\Omega_{fg})$, one obtains the transformation $|g\rangle \to -i|f\rangle$ and $|f\rangle \to -i|g\rangle$ according to Eq. (A2); while the state $|h\rangle$ remains unchanged.

(iv) Apply a classical pulse (with $\phi = \pi/2$) to the ququart. The pulse is resonant with the $|g\rangle \leftrightarrow |f\rangle$ transition. After the pulse duration $\arccos\sqrt{2/3}/\Omega_{fg}$, the transformation $|g\rangle \to \sqrt{\frac{2}{3}}|g\rangle - \sqrt{\frac{1}{3}}|f\rangle$ and $|f\rangle \to \sqrt{\frac{1}{3}}|g\rangle + \sqrt{\frac{2}{3}}|f\rangle$ is achieved according to Eq. (A2); while the state $|h\rangle$ remains unchanged.

(v) Apply a classical pulse (with $\phi = -\pi/2$) to the ququart. The pulse is resonant with the $|f\rangle \leftrightarrow |h\rangle$ transition. After the pulse duration $\pi/(4\Omega_{hf})$, the transformation $|f\rangle \to \frac{1}{\sqrt{2}}(|f\rangle + |h\rangle)$ and $|h\rangle \to \frac{1}{\sqrt{2}}(-|f\rangle + |h\rangle)$ is realized according to Eq. (A4); while the state $|g\rangle$ remains unchanged.

(vi) Apply a classical pulse (with $\phi = \pi/2$) to the ququart. The pulse is resonant with the $|e\rangle \leftrightarrow |h\rangle$ transition. After the pulse duration $\pi/(2\Omega_{he})$, the transformation $|h\rangle \to |e\rangle$ is obtained according to Eq. (A6); while the states $|g\rangle$ and $|f\rangle$ remain unchanged.

The states of the ququart after each basic operation are summarized below:

$$\begin{aligned} |g\rangle &\xrightarrow{\text{(i)}} |g\rangle \xrightarrow{\text{(ii)}} |g\rangle \xrightarrow{\text{(iii)}} -\mathrm{i}|f\rangle \\ &\xrightarrow{\text{(iv)}} -\mathrm{i}\left(\sqrt{\frac{1}{3}}|g\rangle + \sqrt{\frac{2}{3}}|f\rangle\right) \\ &\xrightarrow{\text{(v)}} \frac{-\mathrm{i}}{\sqrt{3}}(|g\rangle + |f\rangle + |h\rangle) \xrightarrow{\text{(vi)}} \frac{-\mathrm{i}}{\sqrt{3}}(|g\rangle + |e\rangle + |f\rangle), \end{aligned} \tag{A9}$$

$$\begin{aligned} |e\rangle &\xrightarrow{\text{(i)}} |h\rangle \xrightarrow{\text{(ii)}} \frac{1}{\sqrt{2}}(|f\rangle + |h\rangle) \xrightarrow{\text{(iii)}} \frac{1}{\sqrt{2}}(-\mathrm{i}|g\rangle + |h\rangle) \\ &\xrightarrow{\text{(iv)}} \frac{-\mathrm{i}}{\sqrt{3}}|g\rangle + \frac{\mathrm{i}}{\sqrt{6}}|f\rangle + \frac{1}{\sqrt{2}}|h\rangle \\ &\xrightarrow{\text{(v)}} \frac{-\mathrm{i}}{\sqrt{3}}(|g\rangle + \omega^2|f\rangle + \omega|h\rangle) \xrightarrow{\text{(vi)}} \frac{-\mathrm{i}}{\sqrt{3}}(|g\rangle + \omega|e\rangle + \omega^2|f\rangle), \end{aligned} \tag{A10}$$

$$|f\rangle \xrightarrow{\text{(i)}} |f\rangle \xrightarrow{\text{(ii)}} \frac{1}{\sqrt{2}}(|f\rangle - |h\rangle) \xrightarrow{\text{(iii)}} \frac{1}{\sqrt{2}}(-\mathrm{i}|g\rangle - |h\rangle)$$
$$\xrightarrow{\text{(iv)}} \frac{-\mathrm{i}}{\sqrt{3}}|g\rangle + \frac{\mathrm{i}}{\sqrt{6}}|f\rangle - \frac{1}{\sqrt{2}}|h\rangle$$
$$\xrightarrow{\text{(v)}} \frac{-\mathrm{i}}{\sqrt{3}}\left(|g\rangle + \omega|f\rangle + \omega^2|h\rangle\right) \xrightarrow{\text{(vi)}} \frac{-\mathrm{i}}{\sqrt{3}}\left(|g\rangle + \omega^2|e\rangle + \omega|f\rangle\right), \tag{A11}$$

where $\omega = \mathrm{e}^{\mathrm{i}2\pi/3}$. Eqs. (A9)–(A11) show that the state transformation (17) in the main text is realized after the above basic operations. From the descriptions given above, one can see that the operation time required for implementing this state transformation is $t_5 = \pi/(2\Omega_{hf}) + \pi/(2\Omega_{fg}) + \pi/\Omega_{he} + \arccos\sqrt{2/3}/\Omega_{fg}$. We remark that although six basic operations are required for the implementation of the state transformation (17), it may not be an experimental challenge because each basic operation can be fast performed due to the use of the ququart-pulse resonant interaction.

References

1. P. W. Show, in: S. Goldwasser (Ed.), Proceedings of the 35th Annual Symposium on FOCS, IEEE Comput. Soc. Press, Los Alamitos, 1994, p. 124
2. L. K. Grover, Quantum mechanics helps in searching for a needle in a haystack, *Phys. Rev. Lett.* 79(2), 325 (1997)
3. A. Steane, Quantum computing, *Rep. Prog. Phys.* 61(2), 117 (1998)
4. N. J. Cerf, M. Bourennane, A. Karlsson, and N. Gisin, Security of quantum key distribution using D-level systems, *Phys. Rev. Lett.* 88(12), 127902 (2002)
5. B. P. Lanyon, M. Barbieri, M. P. Almeida, T. Jennewein, T. C. Ralph, K. J. Resch, G. J. Pryde, J. L. O'Brien, A. Gilchrist, and A. G. White, Simplifying quantum logic using higher dimensional Hilbert spaces, *Nat. Phys.* 5(2), 134 (2009)
6. F. Xu, J. H. Shapiro, and F. N. C. Wong, Experimental fast quantum random number generation using high dimensional entanglement with entropy monitoring, *Optica* 3(11), 1266 (2016)
7. X. M. Hu, J. S. Chen, B. H. Liu, Y. Guo, Y. F. Huang, Z. Q. Zhou, Y. J. Han, C. F. Li, and G. C. Guo, Experimental test of compatibility-loophole-free contextuality with spatially separated entangled qutrits, *Phys. Rev. Lett.* 117(17), 170403 (2016)
8. A. C. Dada, J. Leach, G. S. Buller, M. J. Padgett, and E. Andersson, Experimental high-dimensional two-photon entanglement and violations of generalized Bell inequalities, *Nat. Phys.* 7(9), 677 (2011)
9. M. Krenn, M. Huber, R. Fickler, R. Lapkiewicz, S. Ramelow, and A. Zeilinger, Generation and confirmation of a (100×100)-dimensional entangled quantum system, *Proc. Natl. Acad. Sci. USA* 111(17), 6243 (2014)
10. Y. Zhang, F. S. Roux, T. Konrad, M. Agnew, J. Leach, and A. Forbes, Engineering two-photon high-dimensional states through quantum interference, *Sci. Adv.* 2(2), e1501165 (2016)
11. H. de Riedmatten, I. Marcikic, H. Zbinden, and N. Gisin, Creating high-dimensional time-bin entanglement using mode locked lasers, *Quantum Inf. Comput.* 2(6), 425 (2002)
12. T. Ikuta and H. Takesue, Enhanced violation of the Collins–Gisin–Linden–Massar–Popescu inequality with optimized time-bin-entangled ququarts, *Phys. Rev. A* 93(2), 022307 (2016)
13. Z. Xie, T. Zhong, S. Shrestha, X. Xu, J. Liang, Y. X. Gong, J. C. Bienfang, A. Restelli, J. H. Shapiro, F. N. C. Wong, and C. W. Wong, Harnessing high-dimensional hyper-entanglement through a biphoton frequency comb, *Nat. Photonics* 9(8), 536 (2015)
14. M. Kues, C. Reimer, P. Roztocki, L. R. Cort'es, S. Sciara, B. Wetzel, Y. Zhang, A. Cino, S. T. Chu, B. E. Little, D. J. Moss, L. Caspani, J. Azaña, and R. Morandotti, On-chip generation of high-dimensional entangled quantum states and their coherent control, *Nature* 546(7660), 622 (2017)
15. P. Imany, J. A. Jaramillo-Villegas, O. D. Odele, K. Han, D. E. Leaird, J. M. Lukens, P. Lougovski, M. Qi, and A. M. Weiner, 50-GHz-spaced comb of high-dimensional frequency-bin entangled photons from an on-chip silicon nitride microresonator., *Opt. Express* 26(2), 1825 (2018)
16. C. Schaeff, R. Polster, R. Lapkiewicz, R. Fickler, S. Ramelow, and A. Zeilinger, Scalable fiber integrated source for higher dimensional path-entangled photonic quNits, *Opt. Express* 20(15), 16145 (2012)
17. C. Schaeff, R. Polster, M. Huber, S. Ramelow, and A. Zeilinger, Experimental access to higher-dimensional entangled quantum systems using integrated optics, *Optica* 2(6), 523 (2015)
18. N. Ofek, A. Petrenko, R. Heeres, P. Reinhold, Z. Leghtas, B. Vlastakis, Y. Liu, L. Frunzio, S. M. Girvin, L. Jiang, M. Mirrahimi, M. H. Devoret, and R. J. Schoelkopf, Extending the lifetime of a quantum bit with error correction in superconducting circuits, *Nature* 536(7617), 441 (2016)
19. J. Q. Liao, J. F. Huang, and L. Tian, Generation of macroscopic Schrödinger-cat states in qubit-oscillator systems, *Phys. Rev. A* 93(3), 033853 (2016)
20. T. Hatomura, Shortcuts to adiabatic cat-state generation in bosonic Josephson junctions, *New J. Phys.* 20(1), 015010 (2018)
21. Y. H. Chen, W. Qin, X. Wang, A. Miranowicz, and F. Nori, Shortcuts to adiabaticity for the quantum Rabi model: Efficient generation of giant entangled cat states via parametric amplification, *Phys. Rev. Lett.* 126(2), 023602 (2021)
22. S. Liu, Y. H. Chen, Y. Wang, Y. H. Kang, Z. C. Shi, J. Song, and Y. Xia, Generation of cat states by a weak parametric drive and a transitionless tracking algorithm, *Phys. Rev. A* 106(4), 042430 (2022)
23. C. P. Yang and Z. F. Zheng, Deterministic generation of Greenberger–Horne–Zeilinger entangled states of cat-state qubits in circuit QED, *Opt. Lett.* 43(20), 5126 (2018)
24. Y. Zhang, T. Liu, Y. Yu, and C. P. Yang, Preparation of entangled W states with cat-state qubits in circuit QED, *Quantum Inform. Process.* 19(8), 218 (2020)

25. Y.-H. Chen, W. Qin, X. Wang, A. Miranowicz, and F. Nori, Shortcuts to adiabaticity for the quantum Rabi model: Efficient generation of giant entangled cat states via parametric amplification, *Phys. Rev. Lett.* 126, 023602 (2021)
26. Y.-H. Chen, R. Stassi, W. Qin, A. Miranowicz, and F. Nori, Fault-tolerant multiqubit geometric entangling gates using photonic cat-state qubits, *Phys. Rev. Applied* 18, 024076 (2022)
27. M. Mirrahimi, Z. Leghtas, V. V. Albert, S. Touzard, R. J. Schoelkopf, L. Jiang, and M. H. Devoret, Dynamically protected cat-qubits: A new paradigm for universal quantum compuation, *New J. Phys.* 16(4), 045014 (2014)
28. S. E. Nigg, Deterministic Hadamard gate for microwave cat-state qubits in circuit QED, *Phys. Rev. A* 89(2), 022340 (2014)
29. Y. H. Kang, Y. H. Chen, X. Wang, J. Song, Y. Xia, A. Miranowicz, S. B. Zheng, and F. Nori, Nonadiabatic geometric quantum computation with cat-state qubits via invariant-based reverse engineering, *Phys. Rev. Res.* 4(1), 013233 (2022)
30. C. P. Yang, Q. P. Su, S. B. Zheng, F. Nori, and S. Han, Entangling two oscillators with arbitrary asymmetric initial states, *Phys. Rev. A* 95(5), 052341 (2017)
31. Y. Zhang, X. Zhao, Z. F. Zheng, L. Yu, Q. P. Su, and C. P. Yang, Universal controlled-phase gate with cat-state qubits in circuit QED, *Phys. Rev. A* 96(5), 052317 (2017)
32. Y. J. Fan, Z. F. Zheng, Y. Zhang, D. M. Lu, and C. P. Yang, One step implementation of a multi-target-qubit controlled phase gate with cat-state qubits in circuit QED, *Front. Phys.* 14(2), 21602 (2019)
33. R. W. Heeres, P. Reinhold, N. Ofek, L. Frunzio, L. Jiang, M. H. Devoret, and R. J. Schoelkopf, Implementing a universal gate set on a logical qubit encoded in an oscillator, *Nat. Commun.* 8(1), 94 (2017)
34. A. Grimm, N. E. Frattini, S. Puri, S. O. Mundhada, S. Touzard, M. Mirrahimi, S. M. Girvin, S. Shankar, and M. H. Devoret, Stabilization and operation of a Kerr-cat qubit, *Nature* 584(7820), 205 (2020)
35. C. Wang, Y. Y. Gao, P. Reinhold, R. W. Heeres, N. Ofek, K. Chou, C. Axline, M. Reagor, J. Blumoff, K. M. Sliwa, L. Frunzio, S. M. Girvin, L. Jiang, M. Mirrahimi, M. H. Devoret, and R. J. Schoelkopf, A Schrodinger cat living in two boxes, *Science* 352(6289), 1087 (2016)
36. Z. Wang, Z. Bao, Y. Wu, Y. Li, W. Cai, W. Wang, Y. Ma, T. Cai, X. Han, J. Wang, Y. Song, L. Sun, H. Zhang, and L. Duan, A flying Schrödinger's cat in multipartite entangled states, *Sci. Adv.* 8, eabn1778 (2022)
37. C. P. Yang, S. I. Chu, and S. Han, Possible realization of entanglement, logical gates, and quantum information transfer with superconducting-quantum-interference-device qubits in cavity QED, *Phys. Rev. A* 67(4), 042311 (2003)
38. J. Q. You and F. Nori, Quantum information processing with superconducting qubits in a microwave field, *Phys. Rev. B* 68(6), 064509 (2003)
39. A. Blais, R. S. Huang, A. Wallraff, S. M. Girvin, and R. J. Schoelkopf, Cavity quantum electro-dynamics for superconducting electrical circuits: An architecture for quantum computation, *Phys. Rev. A* 69(6), 062320 (2004)
40. J. Q. You and F. Nori, Atomic physics and quantum optics using superconducting circuits, *Nature* 474(7353), 589 (2011)
41. I. Buluta, S. Ashhab, and F. Nori, Natural and artificial atoms for quantum computation, *Rep. Prog. Phys.* 74(10), 104401 (2011)
42. Z. L. Xiang, S. Ashhab, J. Q. You, and F. Nori, Hybrid quantum circuits: Superconducting circuits interacting with other quantum systems, *Rev. Mod. Phys.* 85(2), 623 (2013)
43. X. Gu, A. F. Kockum, A. Miranowicz, Y. X. Liu, and F. Nori, Microwave photonics with superconducting quantum circuits, *Phys. Rep.* 718–719, 1 (2017)
44. A. P. M. Place, L. V. H. Rodgers, P. Mundada, B. M. Smitham, M. Fitzpatrick, Z. Leng, A. Premkumar, J. Bryon, A. Vrajitoarea, S. Sussman, G. Cheng, T. Madhavan, H. K. Babla, X. H. Le, Y. Gang, B. Jäck, A. Gyenis, N. Yao, R. J. Cava, N. P. de Leon, and A. A. Houck, New material platform for superconducting transmon qubits with coherence times exceeding 0.3 milliseconds, *Nat. Commun.* 12(1), 1779 (2021)
45. S. Kono, J. Pan, M. Chegnizadeh, X. Wang, A. Youssefifi, M. Scigliuzzo, and T. J. Kippenberg, Mechanically induced correlated errors on superconducting qubits with relaxation times exceeding 0.4 milliseconds, arXiv: 2305.02591 (2023)
46. C. Wang, X. Li, H. Xu, Z. Li, J. Wang, Z. Yang, Z. Mi, X. Liang, T. Su, C. Yang, et al., Towards practical quantum computers transmon qubit with a lifetime approaching 0.5 milliseconds, *npj Quantum Inf.* 8, 3 (2022)
47. F. Yan, S. Gustavsson, A. Kamal, J. Birenbaum, A. P. Sears, D. Hover, T. J. Gudmundsen, D. Rosenberg, G. Samach, S. Weber, J. L. Yoder, T. P. Orlando, J. Clarke, A. J. Kerman, and W. D. Oliver, The flux qubit revisited to enhance coherence and reproducibility, *Nat. Commun.* 7(1), 12964 (2016)
48. A. Somoroff, Q. Ficheux, R. A. Mencia, H. N. Xiong, R. Kuzmin, and V. E. Manucharyan, Millisecond coherence in a superconducting qubit, *Phys. Rev. Lett.* 130, 267001 (2023)
49. M. Hofheinz, H. Wang, M. Ansmann, R. C. Bialczak, E. Lucero, M. Neeley, A. D. O'Connell, D. Sank, J. Wenner, J. M. Martinis, and A. N. Cleland, Synthesizing arbitrary quantum states in a superconducting resonator, *Nature* 459(7246), 546 (2009)
50. H. Wang, M. Hofheinz, J. Wenner, M. Ansmann, R. C. Bialczak, M. Lenander, E. Lucero, M. Neeley, A. D. O' Connell, D. Sank, M. Weides, A. N. Cleland, and J. M. Martinis, Improving the coherence time of superconducting coplanar resonators, *Appl. Phys. Lett.* 95(23), 233508 (2009)
51. M. H. Devoret and R. J. Schoelkopf, Superconducting circuits for quantum information: An outlook, *Science* 339(6124), 1169 (2013)
52. P. J. Leek, S. Filipp, P. Maurer, M. Baur, R. Bianchetti, J. M. Fink, M. Goppl, L. Steffen, and A. Wallraff, Using sideband transitions for two-qubit operations in

superconducting circuits, *Phys. Rev. B* 79(18), 180511 (2009)
53. M. Neeley, M. Ansmann, R. C. Bialczak, M. Hofheinz, N. Katz, E. Lucero, A. O'Connell, H. Wang, A. N. Cleland, and J. M. Martinis, Process tomography of quantum memory in a Josephson-phase qubit coupled to a two-level state, *Nat. Phys.* 4(7), 523 (2008)
54. S. B. Zheng and G. C. Guo, Efficient scheme for two-atom entanglement and quantum information processing in cavity QED, *Phys. Rev. Lett.* 85(11), 2392 (2000)
55. A. Sørensen and K. Mølmer, Quantum computation with ions in thermal motion, *Phys. Rev. Lett.* 82(9), 1971 (1999)
56. D. F. V. James and J. Jerke, Effective Hamiltonian theory and its applications in quantum information, *Can. J. Phys.* 85(6), 625 (2007)
57. G. Kirchmair, B. Vlastakis, Z. Leghtas, S. E. Nigg, H. Paik, E. Ginossar, M. Mirrahimi, L. Frunzio, S. M. Girvin, and R. J. Schoelkopf, Observation of quantum state collapse and revival due to the single-photon Kerr effect, *Nature* 495(7440), 205 (2013)
58. B. Vlastakis, G. Kirchmair, Z. Leghtas, S. E. Nigg, L. Frunzio, S. M. Girvin, M. Mirrahimi, M. H. Devoret, and R. J. Schoelkopf, Deterministically encoding quantum information using 100-photon Schrödinger cat states, *Science* 342(6158), 607 (2013)
59. L. Sun, A. Petrenko, Z. Leghtas, B. Vlastakis, G. Kirchmair, K. M. Sliwa, A. Narla, M. Hatridge, S. Shankar, J. Blumoff, L. Frunzio, M. Mirrahimi, M. H. Devoret, and R. J. Schoelkopf, Tracking photon jumps with repeated quantum non demolition parity measurements, *Nature* 511(7510), 444 (2014)
60. B. Vlastakis, A. Petrenko, N. Ofek, L. Sun, Z. Leghtas, K. Sliwa, Y. Liu, M. Hatridge, J. Blumoff, L. Frunzio, M. Mirrahimi, L. Jiang, M. H. Devoret, and R. J. Schoelkopf, Characterizing entanglement of an artificial atom and a cavity cat state with Bell's inequality, *Nat. Commun.* 6(1), 8970 (2015)
61. O. Milul, B. Guttel, U. Goldblatt, S. Hazanov, L. M. Joshi, D. Chausovsky, N. Kahn, E. Çiftyürek, F. Lafont, and S. Rosenblum, A superconducting quantum memory with tens of milliseconds coherence time, arXiv: 2302.06442 (2023)
62. M. Sandberg, C. M. Wilson, F. Persson, T. Bauch, G. Johansson, V. Shumeiko, T. Duty, and P. Delsing, Tuning the field in a microwave resonator faster than the photon lifetime, *Appl. Phys. Lett.* 92(20), 203501 (2008)
63. Z. L. Wang, Y. P. Zhong, L. J. He, H. Wang, J. M. Martinis, A. N. Cleland, and Q. W. Xie, Quantum state characterization of a fast tunable superconducting resonator, *Appl. Phys. Lett.* 102(16), 163503 (2013)
64. E. Jeffrey, D. Sank, J. Y. Mutus, T. C. White, J. Kelly, R. Barends, Y. Chen, Z. Chen, B. Chiaro, A. Dunsworth, A. Megrant, P. J. J. O'Malley, C. Neill, P. Roushan, A. Vainsencher, J. Wenner, A. N. Cleland, and J. M. Martinis, Fast accurate state measurement with superconducting qubits, *Phys. Rev. Lett.* 112(19), 190504 (2014)
65. J. Heinsoo, C. K. Andersen, A. Remm, S. Krinner, T. Walter, Y. Salathé, S. Gasparinetti, J. C. Besse, A. Potočnik, A. Wallraff, and C. Eichler, Rapid high-fidelity multiplexed readout of superconducting qubits, *Phys. Rev. Appl.* 10(3), 034040 (2018)
66. J. R. Johansson, P. D. Nation, and F. Nori, QuTiP: An open-source Python framework for the dynamics of open quantum systems, *Comput. Phys. Commun.* 183(8), 1760 (2012)
67. J. R. Johansson, P. D. Nation, and F. Nori, QuTiP2: A Python framework for the dynamics of open quantum systems, *Comput. Phys. Commun.* 184(4), 1234 (2013)
68. Y. X. Liu, J. Q. You, L. F. Wei, C. P. Sun, and F. Nori, Optical selection rules and phase dependent adiabatic state control in a superconducting quantum circuit, *Phys. Rev. Lett.* 95(8), 087001 (2005)
69. Y. X. Liu, C. X. Yang, H. C. Sun, and X. B. Wang, Coexistence of single- and multi-photon processes due to longitudinal couplings between superconducting flux qubits and external fields, *New J. Phys.* 16(1), 015031 (2014)
70. T. Niemczyk, F. Deppe, H. Huebl, E. P. Menzel, F. Hocke, M. J. Schwarz, J. J. Garcia-Ripoll, D. Zueco, T. Hümmer, E. Solano, A. Marx, and R. Gross, Circuit quantum electrodynamics in the ultrastrong coupling regime, *Nat. Phys.* 6(10), 772 (2010)
71. F. Yoshihara, T. Fuse, S. Ashhab, K. Kakuyanagi, S. Saito, and K. Semba, Superconducting qubit–oscillator circuit beyond the ultrastrong-coupling regime, *Nat. Phys.* 13(1), 44 (2017)
72. F. Yoshihara, T. Fuse, Z. Ao, S. Ashhab, K. Kakuyanagi, S. Saito, T. Aoki, K. Koshino, and K. Semba, Inversion of qubit energy levels in qubit-oscillator circuits in the deep-strong-coupling regime, *Phys. Rev. Lett.* 120(18), 183601 (2018)
73. J. Q. You, X. Hu, S. Ashhab, and F. Nori, Low-decoherence flux qubit, *Phys. Rev. B* 75, 140515(R) (2007)
74. L. V. Abdurakhimov, I. Mahboob, H. Toida, K. Kakuyanagi, and S. Saito, A long-lived capacitively shunted flux qubit embedded in a 3D cavity, *Appl. Phys. Lett.* 115(26), 262601 (2019)
75. C. P. Yang, Q. P. Su, and S. Han, Generation of Greenberger Horne–Zeilinger entangled states of photons in multiple cavities via a superconducting qutrit or an atom through resonant interaction, *Phys. Rev. A* 86(2), 022329 (2012)
76. M. Baur, S. Filipp, R. Bianchetti, J. M. Fink, M. Göppl, L. Steffen, P. J. Leek, A. Blais, and A. Wallraff, Measurement of Autler–Townes and mollow transitions in a strongly driven superconducting qubit, *Phys. Rev. Lett.* 102(24), 243602 (2009)
77. W. Woods, G. Calusine, A. Melville, A. Sevi, E. Golden, D. K. Kim, D. Rosenberg, J. L. Yoder, and W. D. Oliver, Determining interface dielectric losses in superconducting coplanar-waveguide resonators, *Phys. Rev. Appl.* 12(1), 014012 (2019)
78. A. Melville, G. Calusine, W. Woods, K. Serniak, E. Golden, B. M. Niedzielski, D. K. Kim, A. Sevi, J. L. Yoder, E. A. Dauler, and W. D. Oliver, Comparison of dielectric loss in titanium nitride and aluminum superconducting resonators, *Appl. Phys. Lett.* 117(12), 124004 (2020)